

Supplementary Information

Enhancing proline-rich antimicrobial peptide action by homodimerization: Influence of bifunctional linker

Wenyi Li^{1,2*}, Feng Lin³, Andrew Hung⁴, Anders Barlow⁵, Marc-Antoine Sani^{1,6}, Rita Paolini², William Singleton², James Holden², Mohammed Akhter Hossain^{3,6}, Frances Separovic^{1,6}, Neil M. O'Brien-Simpson^{1,2*} and John D. Wade^{3,6*}

¹The Bio21 Institute of Molecular Science and Biotechnology, ²Melbourne Dental School, Centre for Oral Health Research, ³Florey Institute of Neuroscience and Mental Health, University of Melbourne, ⁴School of Science, RMIT University, ⁵Materials Characterisation and Fabrication Platform and ⁶School of Chemistry, University of Melbourne, Victoria 3010, Australia.

*Wenyi Li: wenyi.li@unimelb.edu.au,
Neil O'Brien-Simpson: neil.obs@unimelb.edu.au
John D. Wade: john.wade@florey.edu.au

Contents

Materials	3
The synthesis and bioconjugation of the PrAMPs.....	3
Dimer peptide conjugation with (dibromomethyl)benzene linkers	3
Dimer peptide conjugation with hexafluorobenzene and decafluorobiphenyl linkers	4
Antibacterial assay of the bifunctional linker	5
Minimum membrane disruption concentration (MDC) determination	6
Cell proliferation and lactate dehydrogenase (LDH) determination	6
Therapeutic index (TI).....	7
Bacterial time killing	9
N-phenyl-naphthylamine (NPN) outer membrane permeability	11
Inner membrane permeability	11
Dye leakage assay	14
ROS production determination	17
Peptide stability in bacterial culture	19
Nitric oxide release determination with LPS from <i>A. baumannii</i> ATCC 19606 and FADDI-AB156.....	19
Serum stability	20
Molecular dynamics simulations	22

Materials

9-Fluorenylmethoxycarbonyl (Fmoc)-L-amino acids, 2-(6-chloro-1H-benzotriazole-1-yl)-1,1,3,3-tetramethylammonium hexafluorophosphate (HCTU), and 2-chlorotriyl chloride resin were purchased from GL Biochem (Shanghai, China). TentaGel-MB-RAM-resin was from Rapp Polymere (Tubingen, Germany). N,N-Diisopropylethylamine (DIPEA), dimethylformamide (DMF), Colistin (Aldrich), gentamicin (Aldrich), thiourea (>99%, Aldrich) and trifluoroacetic acid (TFA) were obtained from Auspep (Melbourne, Australia). 1,6-Bimaleimido-hexane was obtained from TCL (Adelaide, Australia). Isobutyl chloroformate (IBCF), α,α' -dibromo-*p*-xylene, piperidine, triisopropylsilane (TIPS), anisole and acetonitrile (CH₃CN) were all obtained from Sigma (Sydney, Australia). Dulbecco's Modified Eagle Medium (DMEM, GIBCO Cat. No. 11995), fetal bovine serum (FBS, GIBCO Cat. No. 10099), SYTO® 9 green fluorescent nucleic acid stain and propidium iodide (PI) were purchased from Invitrogen and used as received. Mueller-Hinton Broth (MHB) (CM0405), and Yeast Extract (LP0021) were purchased from Oxoid. Bacto™ Tryptone and Bacto™ Agar were purchased from BD Biosciences. BacLight Bacterial Membrane Potential Kit (Invitrogen) was used to conduct the membrane potential assay. CellROX® Orange Reagent (Invitrogen) was used to perform the reactive oxygen species (ROS) production assay. 96-well cell culture plates were used for cell culture. Microscope Coverglass (ProSciTech) was used to contain samples for imaging with helium ion microscopy (HIM).

The synthesis and bioconjugation of the PrAMPs

Peptide preparation. The monomeric Chex1-Arg20 with C-terminal Cys and hydrazide (-NHNH₂) modification was synthesized using chloro-(2'-chloro)trityl Polystyrene Resin by Fmoc/tBu solid-phase methods as previously described¹. Standard Fmoc-chemistry was used throughout with a 4-fold molar excess of the Fmoc-protected amino acids in the presence of 3.9-fold HCTU and 10-fold DIPEA. The peptides were cleaved from the solid support resin with TFA in the presence of anisole, TIPS and DODT as the scavenger (ratio 95:2:2:1) for 1 h at room temperature (r.t.). After filtration to remove the resin, the filtrate was concentrated under a stream of nitrogen, and the peptide products were precipitated in ice-cold diethyl ether and washed three times. The peptides were then purified with C18 column (Shimadzu Shim-Pack C18 3.0x75mm) by reversed-phase high performance liquid chromatography (RP-HPLC) in water and acetonitrile containing 0.1% TFA with the gradient 0-80% of buffer B (acetonitrile) at 1.2 mL/min. The final products were characterized by both Shimadzu RP-HPLC and Shimadzu matrix-assisted laser desorption/ionization time-of-flight mass spectrometry (MALDI-TOF MS).

Dimer peptide conjugation with (dibromomethyl)benzene linkers

To a solution of monomeric PrAMP-NHNH₂ (7.7 μ mol) in 0.1%TFA (40 μ L) and 1 M zinc acetate (36.8 μ mol, 36.8 μ l) was added dropwise a 20 mM solution of linker including (1,2-dibromomethyl-benzene, 1,3-dibromomethyl-benzene, 1,4-dibromomethyl-benzene) that was dissolved in acetonitrile (3.5 μ mol, 175 μ L). The mixture was reacted for 2-6 h at r.t. and the crude peptides were purified by RP-HPLC in water and acetonitrile containing 0.1% TFA in overall moderate yield (Table S1). The final products were characterized by both RP-HPLC and MALDI-TOF MS (Figure S1).

Dimer peptide conjugation with hexafluorobenzene and decafluorobiphenyl linkers

To a solution of monomeric PrAMP- NHHNH₂ (5.4 μmol) and 4-(dimethylamino)pyridine (53 μmol, 6.5 mg) in DMF (30 μL) was added dropwise a 20 mM solution of linker including (hexafluorobenzene, decafluorobiphenyl) that was dissolved in DMF (2.2 μmol, 110 μL). The mixture was reacted overnight at r.t. and the crude peptides were purified by RP-HPLC in water and acetonitrile containing 0.1% TFA in overall moderate yield (Table S1). The final products were characterized by both RP-HPLC and MALDI-TOF MS (Figure S1).

Table S1 The preparation and yield of the tested PrAMPs.

	Peptides	linkers	Yield (%)	Purity
1	Monomer-NHHNH ₂		56.3	94.89%
2	disulfide dimer-NHHNH ₂	disulfide bond	45.6	97.3%
3	p-Xylene dimer-NHHNH ₂	p-(1,4)-dibromomethylbenzene	46.8	93.69%
4	o-Xylene dimer-NHHNH ₂	o-(1,3)-dibromomethylbenzene	22.2	98.76%
5	m-Xylene dimer-NHHNH ₂	m-(1,2)-dibromomethylbenzene	40.5	95.47%
6	Tetrafluorobenzene dimer-NHHNH ₂	hexafluorobenzene	22.1	95.63%
7	Octofluorobiphenyl dimer-NHHNH ₂	Decafluorobiphenyl	27.9	94.22%

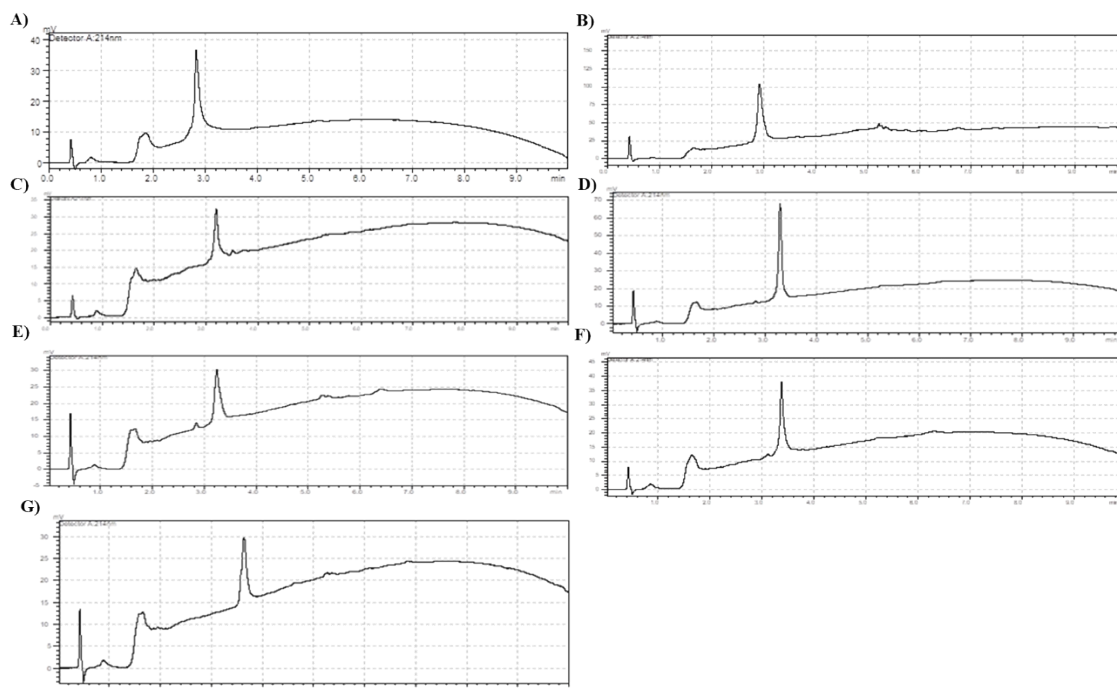


Figure S1. Characterization of synthetic PrAMPs. A) Monomer-NHNH₂, 1; Calculated MS: 2650.96, ESI MS: 2649.5238; B) disulfide dimer-NHNH₂, Calculated MS: 5185.92, ESI MS: 5185.0033; 2; C) *p*-Xylene dimer-NHNH₂, Calculated MS: 5289.08, ESI MS: 5288.0463; 3; D) *o*-Xylene dimer-NHNH₂, Calculated MS: 5289.08, ESI MS: 5290.0164; 4; E) *m*-Xylene dimer-NHNH₂, Calculated MS: 5289.08, ESI MS: 5289.0651; 5; F) Tetrafluorobenzene dimer-NHNH₂, Calculated MS: 5332.97, ESI MS: 5332.9820; 6; G) Octofluorobiphenyl dimer-NHNH₂, 7, Calculated MS: 5481.03, ESI MS: 5480.9760.

Antibacterial assay of the bifunctional linker

To observe the effects of the bifunctional linker on the antibacterial activity, antibacterial assays using the two linkers, hexafluorobenzene and decafluorobiphenyl, were performed against a panel of Gram-negative bacteria, including *Escherichia coli* ATCC 25922, *Klebsiella pneumoniae* ATCC 13883, *Acinetobacter baumannii* ATCC 19606, as well as the multi-drug resistant (MDR) *K. pneumoniae* FADDI-KP028 and MDR *A. baumannii* FADDI-AB156 (colistin-resistant, rifampin-resistant & MDR) (Table S2).

Table S2 Antibacterial activity effect of linker (MIC). All data were performed two times in duplicate and determined as mean \pm standard deviation.

Linker ($\mu\text{g/mL}$)	<i>E. coli</i> 25922	<i>K.</i> <i>pneumoniae</i> 13883	<i>A.</i> <i>baumannii</i> 19606	FADDI- KP028	FADDI- AB156
Hexafluorobenzene	>250	>250	>250	>250	>250
Decafluorobiphenyl	>250	>250	>250	>250	>250

Minimum membrane disruption concentration (MDC) determination

To determine the membrane integrity, the DNA fluorescent dyes propidium iodide (PI) and SYTO 9 were applied to monitor the effects of the PrAMPs using microbial MPs to monitor as previously described^{2, 3}. Briefly, a series of 100 µl PrAMP solutions diluted from 250 µg/mL to 4 µg/mL were added to a 96-well plate with pre-filled 100 µl of 2×10^6 cells/mL. After 90 min incubation at 37°C, 50 µl of the culture mixture were transferred to a new 96-well plate and mixed with 50 µl mixture of PI (1.67 µM) and SYTO 9 (0.83 µM) in phosphate buffered saline (PBS). Then the plate was subjected to flow cytometric analysis via CytoFLEX LX Flow Cytometer (Beckman Coulter) with the channel setting of SYTO 9 (Blue channel 525-40 nm, bacterial population with intact membrane) and PI (Yellow/Green channel 610-20 nm, bacterial population without intact membrane). The MDC values were determined by the concentration of PrAMP resulting in over 90% PI positive labelling of bacterial population under CytoFLEX LX Flow Cytometer.

Table S3 Minimum membrane disruption concentration (MDC) (µg/mL). All data are performed twice in duplicate and determined as mean ± standard deviation.

	Peptides	<i>E. coli</i> 25922	<i>K. pneumoniae</i> 13883	<i>A. baumannii</i> 19606
1	Monomer- NHNH ₂	>250	>250	>250
2	disulfide dimer-NHNH ₂	30.9±1.4	8.3±0.3	43.9±1.0
3	p-Xylene dimer-NHNH ₂	11.8±0.6	17.5±0.1	21.1±0.6
4	o-Xylene dimer-NHNH ₂	19.1±0.2	18.1±2.0	25.7±1.0
5	m-Xylene dimer-NHNH ₂	19.8±0.8	32.7±1.4	23.7±0.7
6	Tetrafluorobenzene dimer- NHNH ₂	6.2±0.5	6.9±0.2	10.6±0.5
7	Octofluorobiphenyl dimer- NHNH ₂	4.1±0.1	4.2±0.1	4.5±0.1

Cell proliferation and lactate dehydrogenase (LDH) determination

The proliferation and LDH of HEK-293 (ATCC® CRL-1573™) cells were determined by using CellTiter 96 AQueous Non-Radioactive Cell Proliferation Assay and CytoTox 96® Non-Radioactive Cytotoxicity Assay (Promega) as described previously⁴. Briefly, 5×10^3 cells (100 µl) and PrAMPs at different concentration (from 125 µg/mL to 0.2 µg/mL) were seeded into 96-well plates and cultured overnight at 37°C, 5% CO₂. After incubation, 50 µl of the supernatant from each well was transferred to a new 96 well flat bottom plate, followed by the addition of 50 µl LDH solution for 30 min incubation at r.t. After the addition of 50 µl stop solution, the plate was subjected to record absorbance at 490 nm. The LDH generation from the cell samples were calculated as follows (Figure S2):

$$C_{ytotoxicity} \% = \frac{\text{Experimental LDH Release (OD490)}}{\text{Maximum LDH Release (OD490)}} \times 100$$

After the LDH test in 96 well plate, 20 μ l of the solution with tetrazolium compound [3-(4,5-dimethylthiazol-2-yl)-5-(3-carboxymethoxyphenyl)-2-(4-sulfophenyl)-2H-tetrazolium, inner salt; MTS] and an electron coupling reagent (phenazine methosulfate) PMS were added to each well followed by 1 h incubation at 37°C, 5% CO₂. The plate was then subjected to record absorbance at 490 nm. The proliferation effects of PrAMPs on HEK cells were calculated as followed (Figure S2):

$$\text{Viable cells \%} = \frac{\text{Experimental viable cells (OD490)}}{\text{Maximum viable cells (OD490)}} \times 100$$

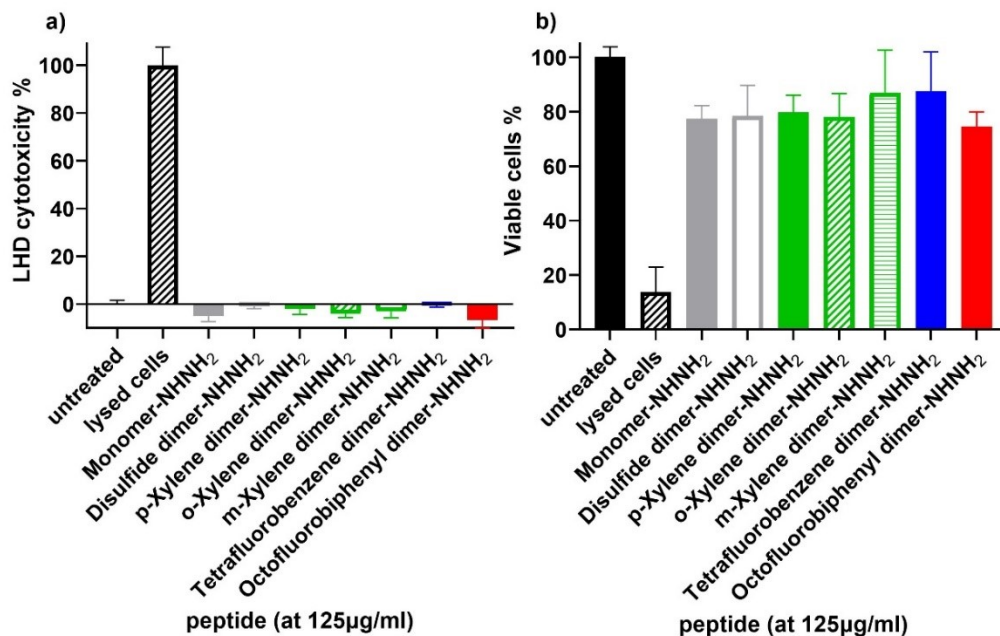


Figure S2. Cytotoxicity against HEK 273 cells. a) LDH cytotoxicity of PrAMPs at the highest tested concentration (125 µg/mL). b) Cell proliferation of PrAMPs at the highest tested concentration (125 µg/mL). All data are performed twice in duplicate and determined as mean \pm standard deviation.

Therapeutic index (TI)

The safety profile of the PrAMPs was determined using the calculated TI. As the MIC (Table 1) and cytotoxicity (Figure S2) were determined, the TI was calculated with the formula as IC₅₀/MIC₅₀. Since all the PrAMPs did not show any significant toxicity towards HEK-293 (ATCC® CRL-1573™) cells, the TI can only be calculated as the minimum index (Table S4). The weight-of-evidence approach and bioactivity parameters suggest the PrAMPs display a more balanced safety–efficacy profile.

Table S4. Therapeutic Index (TI) for *A. baumannii* 19606 and FADDI-AB156.

	Peptides	<i>A. baumannii</i> 19606			<i>FADDI-AB156</i>		
		MIC ₅₀	IC ₅₀	TI=IC ₅₀ /MIC ₅₀	MIC ₅₀	IC ₅₀	TI=IC ₅₀ /MIC ₅₀
1	monomer- NHHNH ₂	125	>125	>1	200	>125	>0.6
2	disulfide dimer- NHHNH ₂	25.9±1 .8	>125	>4.8	16.6±3 .1	>125	>7.5
3	p-Xylene dimer- NHHNH ₂	7.4±0. 8	>125	>16.8	31.3±1 .8	>125	>4
4	o-Xylene dimer- NHHNH ₂	10.0±1 .4	>125	>12.5	31.1±0 .1	>125	>4
5	m-Xylene dimer- NHHNH ₂	7.4±0. 9	>125	>16.9	31.6±0 .3	>125	>4
6	Tetrafluorobenzene dimer- NHHNH ₂	3.3±0. 1	>125	>37.9	7.6±0. 2	>125	>16
7	Octofluorobiphenyl dimer- NHHNH ₂	3.5±0. 3	>125	>35.7	4.1±0. 2	>125	>30

Bacterial time killing

Bactericidal time killing efficiency of the PrAMPs was determined against *A. baumannii* and MDR-FADDI-AB156. The mid-logarithmic phase bacterial cells were re-suspended into MHB of 2×10^6 cells/mL and then 100 μ L bacteria were incubated with PrAMPs at different concentration ($4 \times \text{MIC}$, $2 \times \text{MIC}$, $1 \times \text{MIC}$, $0.5 \times \text{MIC}$, $0.25 \times \text{MIC}$) at 37°C . 10 μ L of aliquot was removed from the treated bacterial suspension at specific time intervals (0, 5, 10, 20, 30, 45, 60, 75 and 90 min) and plated on the LB-agar plates to determine the colony-forming units (CFU) at each time point after overnight incubation (Figure S3).

Based on the CFU count at various time points, the first order death rate constant was determined by plotting $\text{Log}(\text{CFU})$ vs. time range from 5-60 min⁵ (Figure S4). The regression of the linear fit was obtained with Graphpad and the slope of linear fit provided the death rate constant (Figure S4). Then the death rate constants obtained from Figure S4 were subject of the plot for death rate constant vs. peptide concentration in Figure 2.

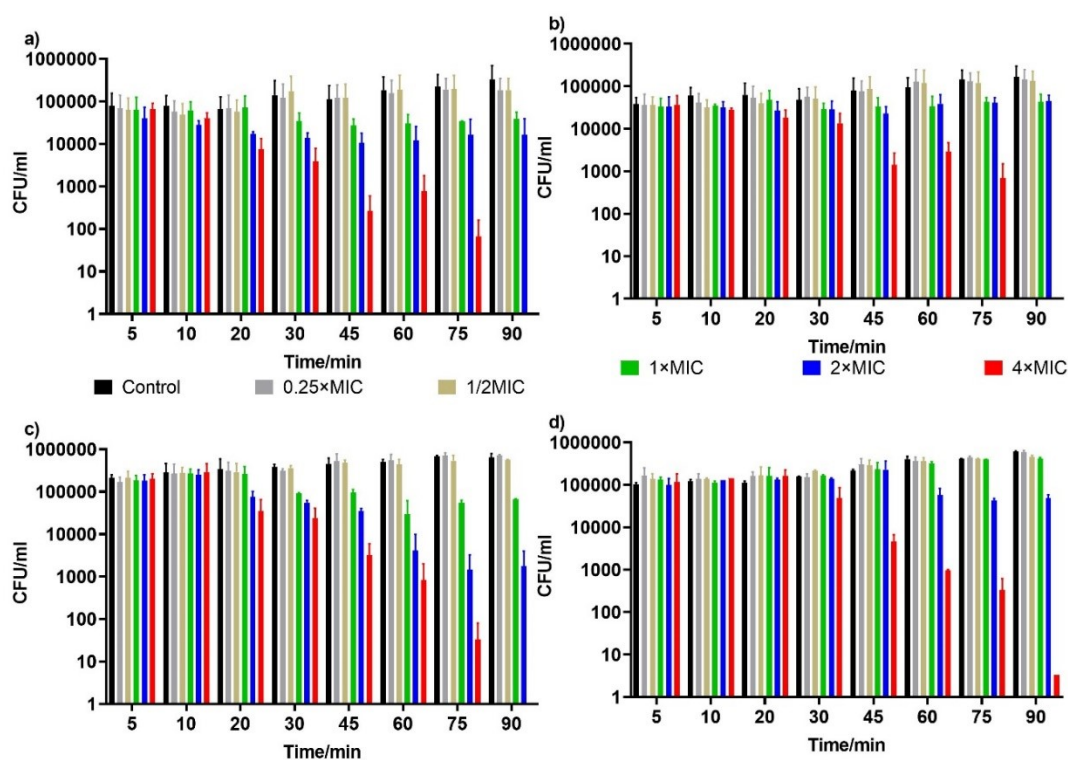


Figure S3. Time killing-kinetic assays for lead PrAMPs against *A. baumannii* and MDR-FADDI-AB156. Survival of (a) *A. baumannii* and (c) MDR-FADDI-AB156 incubated with tetrafluorobenzene dimer-NH₂ 6 at differing times and concentrations. Survival of (b) *A. baumannii* and (d) MDR-FADDI-AB156 incubated with octofluorobiphenyl dimer-NH₂ 7 at differing times and concentrations. Data representative of 2 biological replicates with 2 technical replicates/assay.

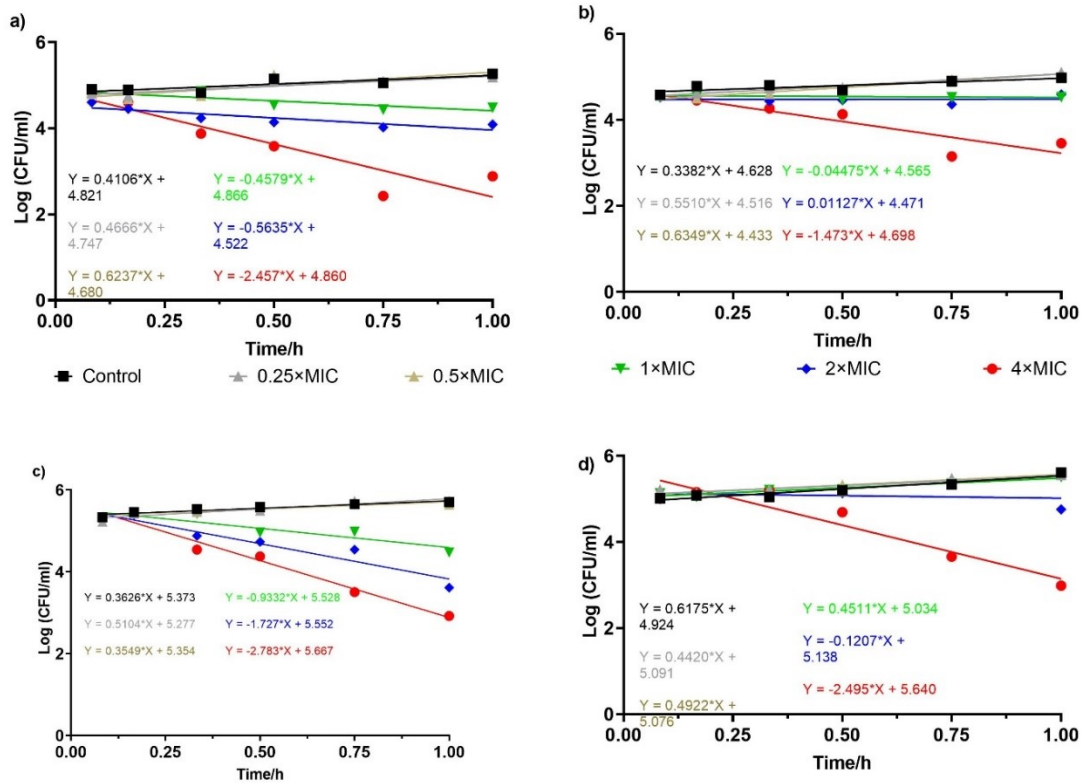


Figure S4. The first order death rate constant was determined by plotting Log(CFU) vs. time (a) *A. baumannii* and (c) MDR-FADDI-AB156 incubated with tetrafluorobenzene dimer-NHNH₂ 6 at differing concentrations with the bacteria only (black), 0.25 × MIC PrAMP 6 (gray), 0.5 × MIC PrAMP 6 (golden), 1 × MIC PrAMP 6 (green), 2 × MIC PrAMP 6 (blue), and 4 × MIC PrAMP 6 (red). (b) *A. baumannii* and (d) MDR-FADDI-AB156 incubated with octofluorobiphenyl dimer-NHNH₂ 7 at differing concentrations labelled in colours. The death rate constants vs. concentration are plotted in Figure 2.

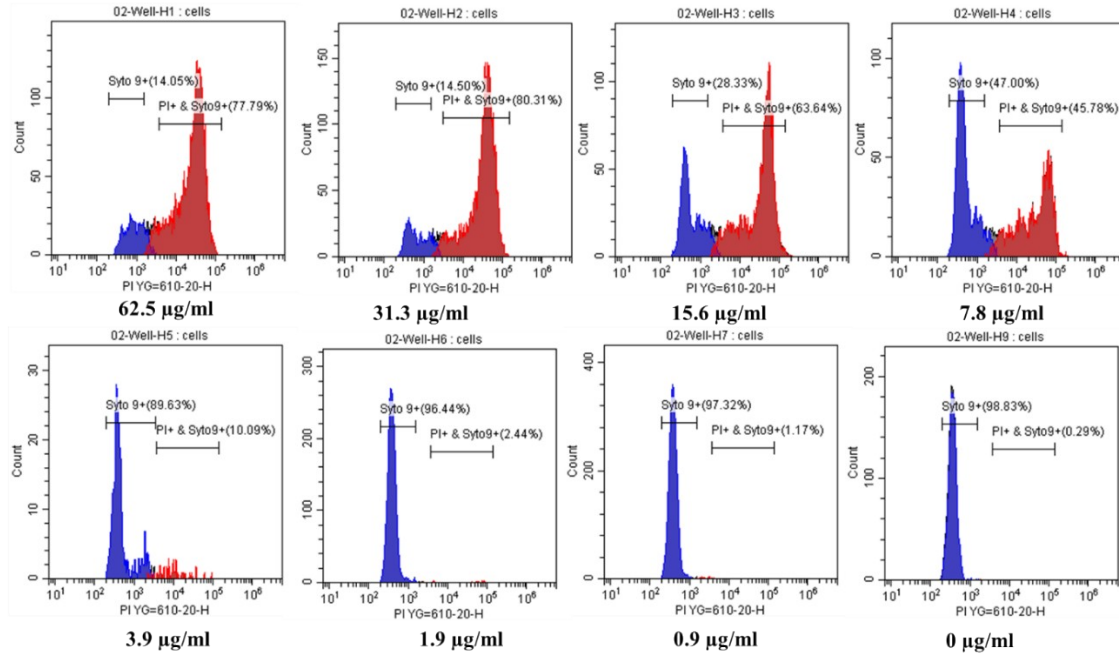
N-phenyl-naphthylamine (NPN) outer membrane permeability

Based on the N-phenyl-naphthylamine (NPN) fluorescence property while in contact with a phospholipid bilayer⁶, the outer membrane permeability was determined at different concentrations of the lead PrAMPs. Briefly, the bacterial culture at exponential phase ($OD = 0.5$) was harvested at 3500 rpm (10 min, r.t.) and resuspended into HEPES buffer (1 mM, pH 7.2) into OD_{600} of 0.5. The 50 μ l of a series concentration of PrAMPs ($2\times MIC$, $1\times MIC$, $0.5\times MIC$, $0.25\times MIC$, $0.1\times MIC$) were added to a 96-well plate prefilled with 100 μ l bacterial culture (in HEPES buffer), followed by the addition of 50 μ l of NPN (40 μ M, final concentration of 10 μ M). Meanwhile, due to the potent permeability of polymyxin B⁷, a triple well with polymyxin B (6.4 μ g/mL) was prepared as the positive control. After 10 min incubation, the plate was measured at 355/405 nm by using a fluorescence spectrophotometer (PerkinElmer 1420 Multilabel Counter VICTOR). The fluorescence intensity of each treated sample was compared with the positive control of polymyxin B as shown in Figure 3.

Inner membrane permeability

Since the inner membrane is impermeable to PI, it has been used to differentiate the membrane integrity under different treatments, while SYTO 9 penetrates all cell membranes. In this assay, 100 μ l of diluted PrAMPs from 62.5 μ g/mL to 0.9 μ g/mL were added to 100 μ l of 2×10^6 cells/mL in a 96-well plate. After 60 min incubation at 37°C, 50 μ l of the culture mixture was transferred to a new 96-well plate and mixed with 50 μ l mixture of PI (1.67 μ M) and SYTO 9 (0.83 μ M) in PBS. Then the plates were subjected to flow cytometric analysis via CytoFLEX LX Flow Cytometer (Beckman Coulter), with the SYTO 9 labelled bacterial population with the intact membrane (blue coloured) and PI-labelled bacterial population for PrAMPs with inner membrane penetration (red coloured) (Figure S5 & Figure S6). The inner membrane permeability of PrAMPs were plotted as PI-labelled population (Figure 4).

Tetrafluorobenzene dimer-hydraide against *A. baumannii*



Octofluorobiphenyl dimer-hydraide against *A. baumannii*

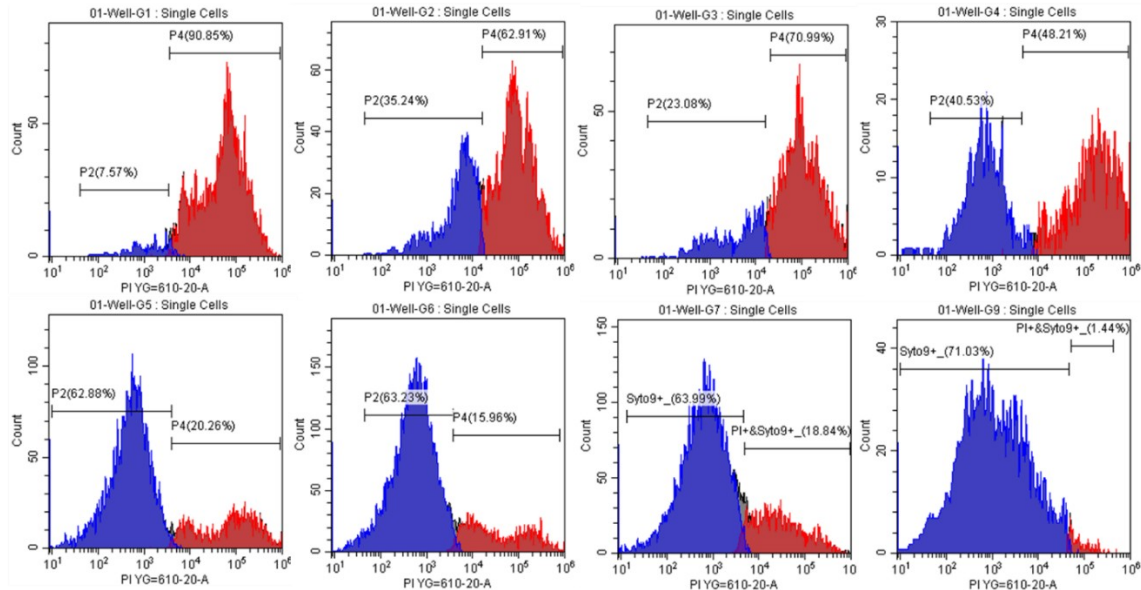
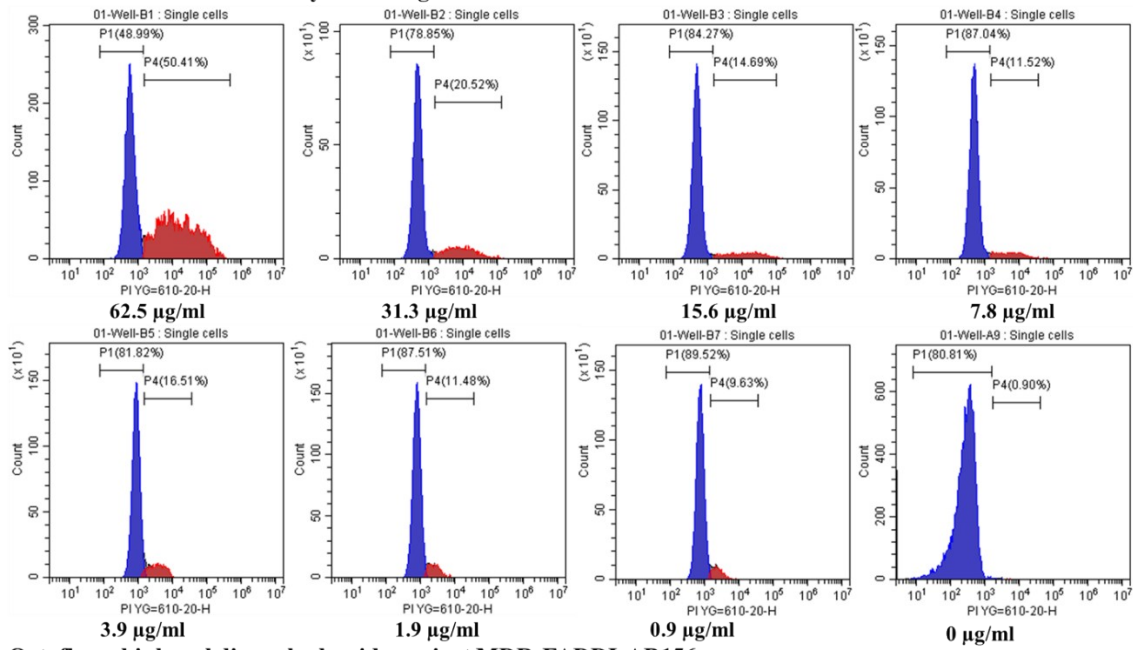


Figure S5. Flow cytometric analysis of PrAMP-treated *A. baumannii*. Untreated samples were used as controls to show the untreated membrane population. Blue colour in each panel represents the SYTO 9-labelled bacterial population, while a red colour indicates inner membrane permeability by PrAMPs with PI-labelled bacterial population.

Tetrafluorobenzene dimer-hydraide against MDR-FADDI-AB156



Octafluorobiphenyl dimer-hydraide against MDR-FADDI-AB156

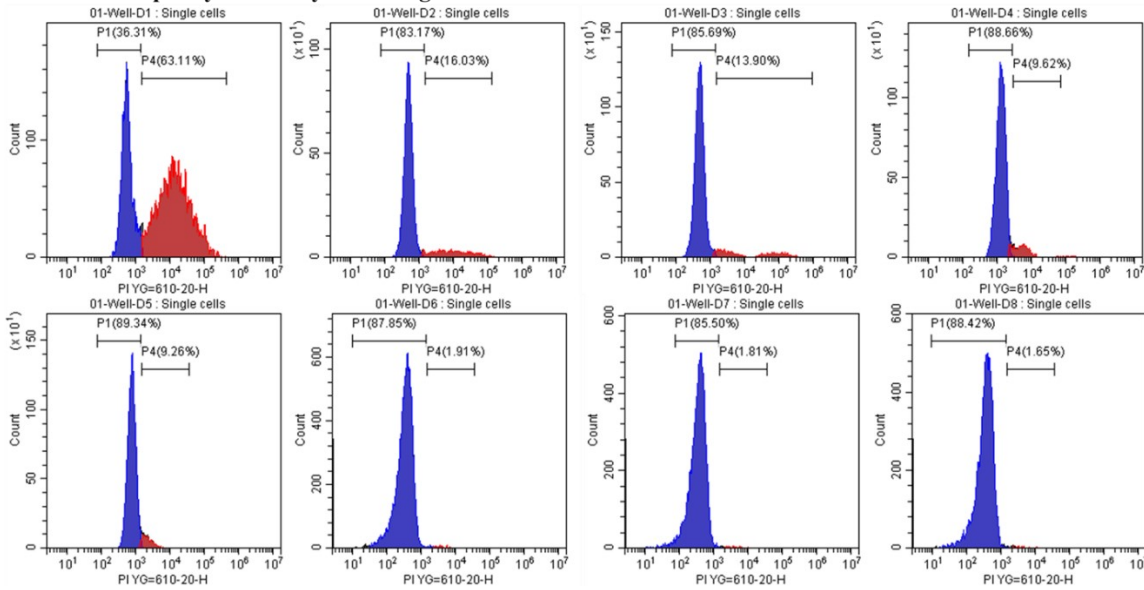


Figure S6. Flow cytometric analysis of PrAMP-treated MDR-FADDI-AB156. Untreated samples were used as control to show the untreated membrane population. Blue colour in each panel indicates the SYTO 9-labelled bacterial population, while red colour indicate inner membrane permeability by PrAMPs with PI-labelled bacterial population.

Dye leakage assay

Large unilamellar vesicles (LUVs) were prepared to mimic bacterial membranes, Phosphatidylglycerol (PG): cardiolipin (9:1) were used to mimic a Gram-positive bacterial membrane and phosphatidylethanolamine (PE): PG (7:3) used to represent a Gram-negative bacterial membrane, as previously described^{8,9}. Using an Avanti Mini-Extruder with 100 nm diameter pore-size polycarbonate filter, LUVs with encapsulated calcein for dye leakage experiments were produced in 20 mM phosphate buffer (with 5 mM NaCl and 0.5 mM ethylenediaminetetraacetic acid (EDTA), pH 7.4) by extrusion at r.t. Calcein leakage was measured using a 96-well plate with a fluorescence plate reader at wavelength 485/535 nm with 3 cycles at 25°C. The fluorescence intensities were averaged and percentage calcein fluorescence calculated *via* the following equation:

$$\text{Fluorescence \%} = \frac{(I - I_n)}{I_p - I_n} \times 100\%$$

in which I represent the fluorescence of LUVs with peptides, I_n represents the fluorescence of the LUVs only, as negative control, and I_p represents the fluorescence of the LUVs with 2% Triton X-100 as the positive control. Then, the normalised intensities were plotted against the lipid to peptide molar ratio (L/P) (Figure S7).

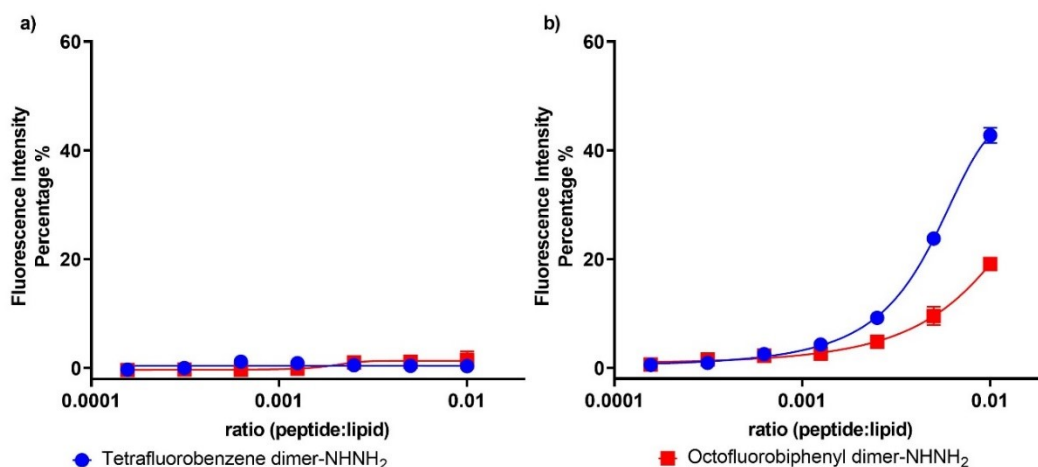


Figure S7. Dye leakage assay. a) phosphatidylglycerol (PG): cardiolipin (9:1) was used to mimic a Gram-positive bacterial membrane, and b) phosphatidylethanolamine (PE): PG (7:3) was used to represent a Gram-negative bacterial membrane. Positive control was treated with 2% Triton X-100. Assays were performed twice in duplicate and plotted as mean \pm standard deviation. Membrane potential assay

The effects of the lead PrAMPs on membrane potential were assessed using a BacLight Bacterial Membrane Potential Kit (Invitrogen) by flow cytometric analysis (CytoFLEX Flow Cytometer, Beckman Coulter). Briefly, 100 μ L of bacterial culture (2×10^6 cells/mL) in MHB was mixed with 100 μ L serial dilution of lead PrAMPs (0.125 \times MBC, 0.25 \times MBC, 0.5 \times MBC, 1 \times MBC, 2 \times MBC) in a 96-well plate. After 60 min incubation at 37°C, the 3,3'-diethyl-oxa-carbocyanine iodide (diOC₂3) (30 μ M) was added to the tested samples and then the plate was subjected to flow cytometric analysis via CytoFLEX LX

Flow Cytometer (Beckman Coulter). Meanwhile, the protonophore, carbonyl cyanide-*m*-chlorophenylhydrazone (CCCP, final concentration 5 μ M), treated sample acted as a depolarized population control. Based on the CCCP control and normal cell samples, gates were drawn to present normal cell population or depolarized regions (Figure S8 & Figure S9).

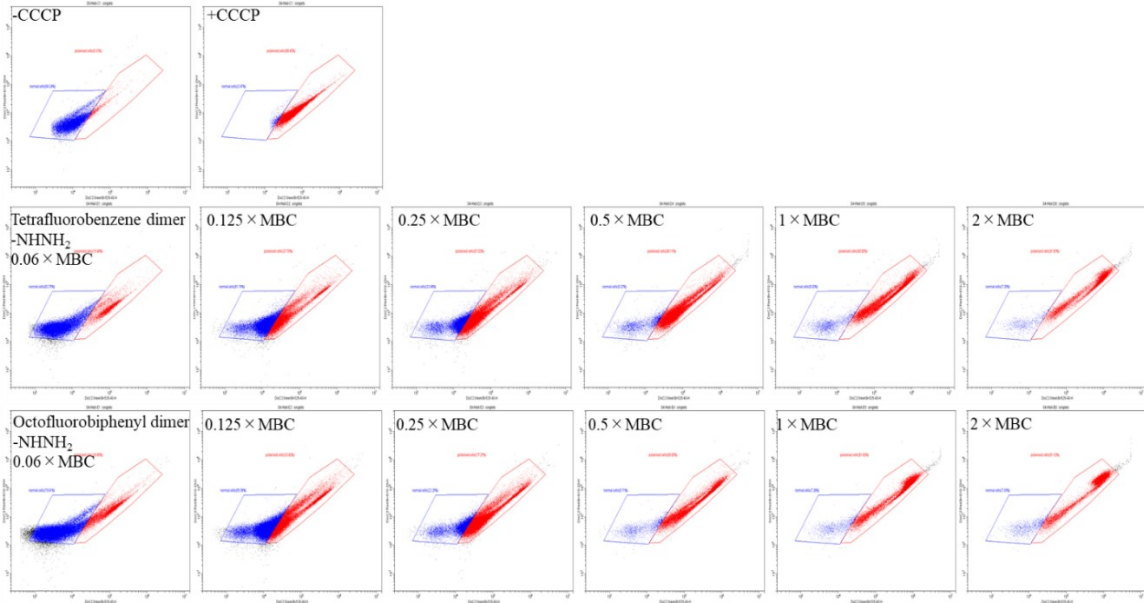


Figure S8. The membrane potential of *A. baumannii* was analysed via flow cytometry. The red population represents depolarised bacteria and the blue population indicates the untreated stage of the bacteria.

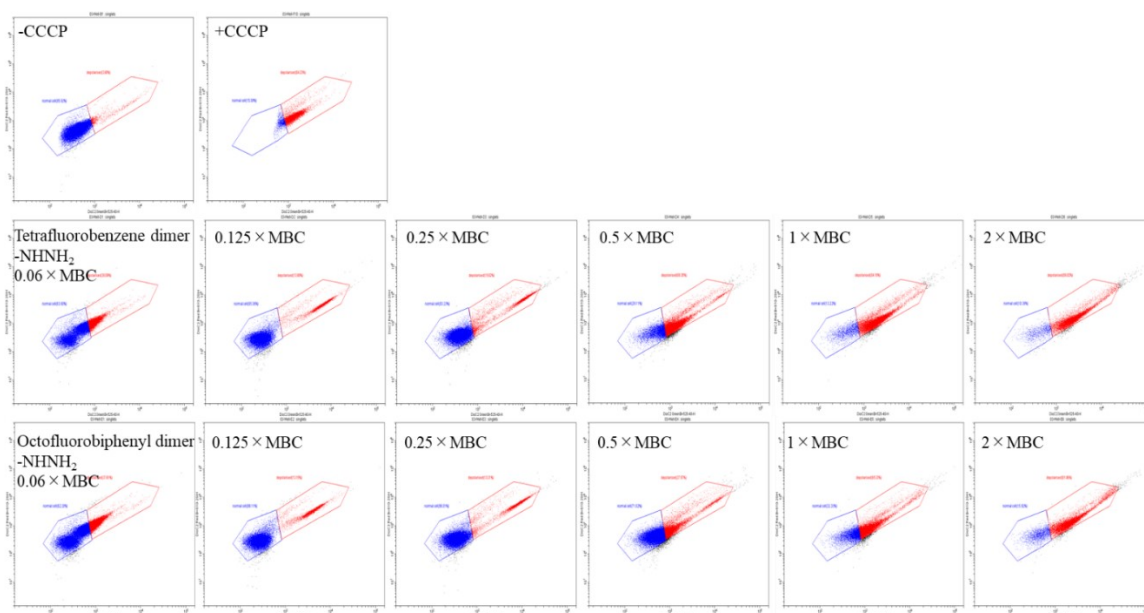


Figure S9. The membrane potential of FADDI-AB156 analysed via flow cytometry. The red population represents depolarised bacteria and blue population indicates untreated stage of the bacteria.

ROS production determination

ROS production from the lead PrAMPs was determined by CellROX deep red reagent by flow cytometric analysis. Briefly, 100 μL of bacterial culture (2×10^6 cells/mL) in DMEM was mixed with 100 μL serial diluted of lead PrAMPs ($0.125 \times \text{MBC}$, $0.25 \times \text{MBC}$, $0.5 \times \text{MBC}$, $1 \times \text{MBC}$, $2 \times \text{MBC}$) in a 96-well plate. After 90 min incubation at 37°C , the bacterial culture was then stained with a mixture of CellROX deep red reagent ($5 \mu\text{M}$) and SYTO 9 reagent ($0.83 \mu\text{M}$), which was then subjected to CytoFLEX Flow Cytometer (Beckman Coulter) analysis. Additionally, the ROS scavenger¹⁰, thiourea, was added to the PrAMPs treated samples as the confirmation for the ROS generation. based on the untreated bacteria, gates were determined during the flow cytometric analysis (Figure S10 & Figure S11). The level of ROS production was plotted at different concentrations (Figure 5).

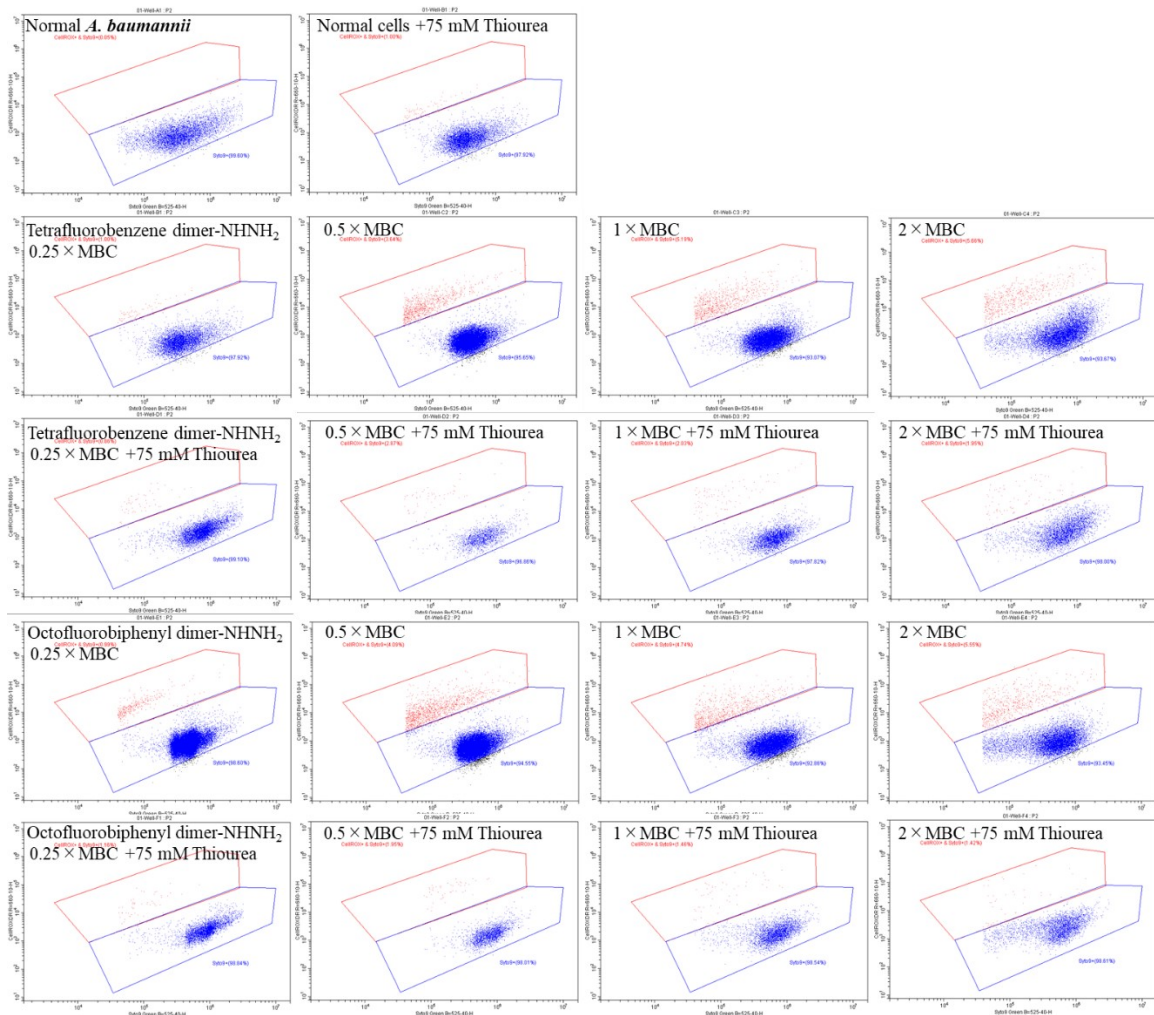


Figure S10. Reactive oxygen species of *A. baumannii* in presence of PrAMPs. The untreated samples were used as controls to show normal cells without significant ROS generation. A blue square in flow cytometry gate indicated the SYTO 9-labelled bacterial population, while a red square indicated the fluorescent dye CellROX deep red reagent labelled bacterial population with ROS generation.

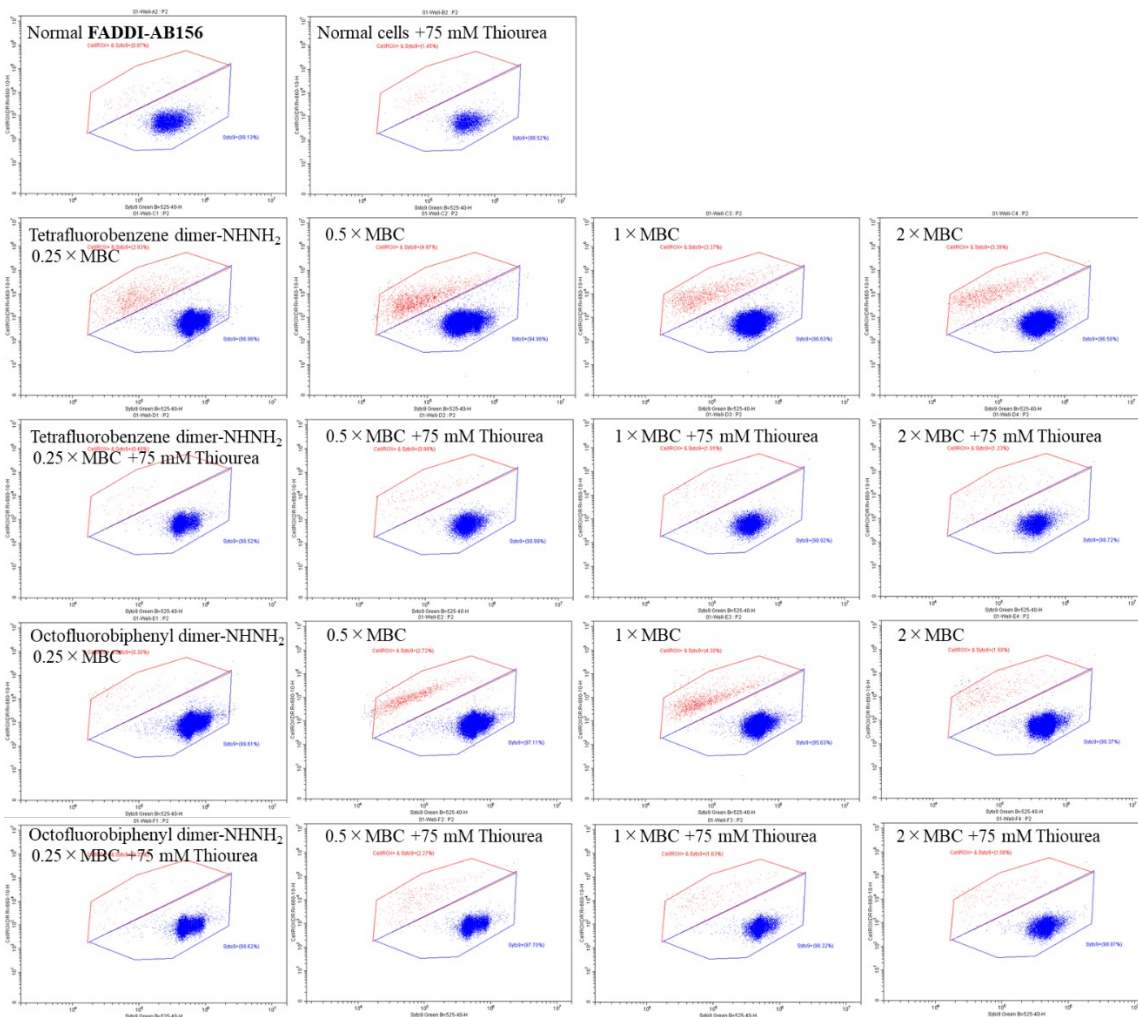


Figure S11. Reactive oxygen species of FADDI-AB156 in presence of PrAMPs. The untreated samples were used as controls to show normal cells without significant ROS generation. A blue square in flow cytometry gate indicated the SYTO 9-labelled bacterial population, while a red square of flow cytometry gate indicated the fluorescent dye CellROX deep red reagent labelled bacterial population with ROS generation.

Peptide stability in bacterial culture

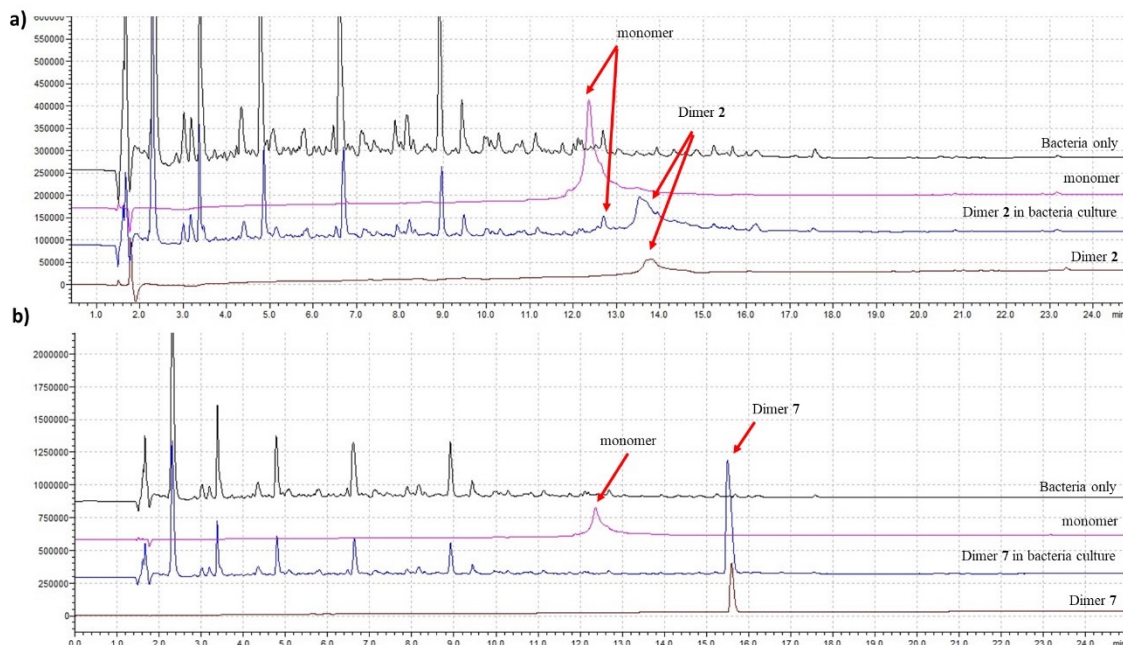


Figure S12. RP-HPLC trace of the disulfide dimer-NHNH₂ 2 (a) and octafluorobiphenyl dimer-NHNH₂ 7 (b) in presence of *A. baumannii* culture after 90 min incubation.

Nitric oxide release determination with LPS from *A. baumannii* ATCC 19606 and FADDI-AB156

Though the commercially available *E. coli* LPS is commonly used to stimulate macrophage cells, the LPS originating from *A. baumannii* ATCC 19606 and FADDI-AB156 from the laboratory cultured bacteria were pursued with adaption from the Tri-Reagent method¹¹. Briefly, the bacterial culture was centrifuged to pellet at 5000 g, 15 min at 4°C. The pellet was suspended into Tri-Reagent (5 mL) for 10 min at r.t. followed by chloroform (500 µl) extraction. The organic phase was further extracted two times with MilliQ water. Then all three aqueous extracts were combined into a 50 mL Falcon tube, followed by the addition of 40 µl DNase/RNase/Lipdase (stock 10 mg/mL) and incubation for 2 h at r.t. To precipitate the LPS, two equivalents of the volume of MgCl₂ (0.375 M in ethanol) was added and kept at -20°C overnight. The precipitates of *A. baumannii* ATCC 19606 and FADDI-AB156 LPS were obtained after centrifugation and lyophilisation for further usage.

Using the extracted the LPS from *A. baumannii* ATCC 19606 and FADDI-AB156, the NO released from RAW264.7 cells was determined with a diluted LPS series. In brief, 100 µl of 1×10⁶ RAW264.7 cells/mL was seeded into a flat-bottom 96-well plate for 24 h at 37°C with 5% CO₂ in DMEM. Then, a series of 50µl/well diluted LPS in DMEM, from 200 µg/mL to 0.05 µg/mL, was added followed by the addition of 100 µl DMEM to give a total of 250 µl in each well. After overnight incubation at 37°C, the culture supernatant (50 µl) was collected for NO concentration determination using a Promega Griess Reagent Kit to measure the absorption with a filter of 540 nm (Figure S13). The concentration of NO in µM (Figure S13) was calculated via the nitrate standard curve (Figure S14).

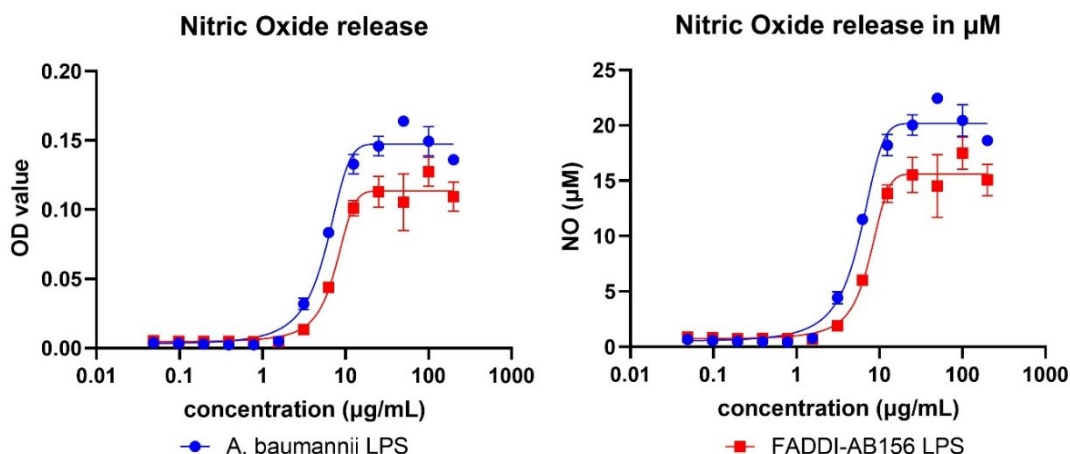


Figure S13. Stimulated NO release from RAW 264.7 by different concentrations of purified LPS from *A. baumannii* and MDR-FADDI-AB156.

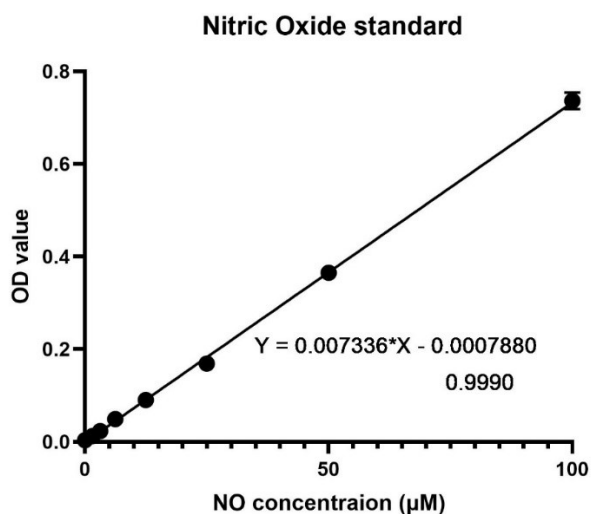


Figure S14. Standard curve for nitric oxide.

Serum stability

Proteolytic stability of the PrAMPs was assessed by incubating the A3-APO (0.1 µg/µl) in a solution of 15% human serum in PBS (pH 7.4) at 37°C, 0.0004% (v:v) 4-isopropylbenzyl alcohol as an internal standard. 15 µl of sample was removed at various time points (0 h, 2 h, 4 h, 6 h and 8 h), and 30 µl of acetonitrile was added to precipitate plasma proteins, which were removed by centrifugation (6200 rpm, 2 mins). The amount of intact PrAMPs remaining in the supernatant of each sample was determined by RP-HPLC, by measuring the area under the peak at appropriate retention time compared to the peak area of PrAMPs at time zero (100%). Then the percentage of intact PrAMPs was plotted vs. time (Figure S15).

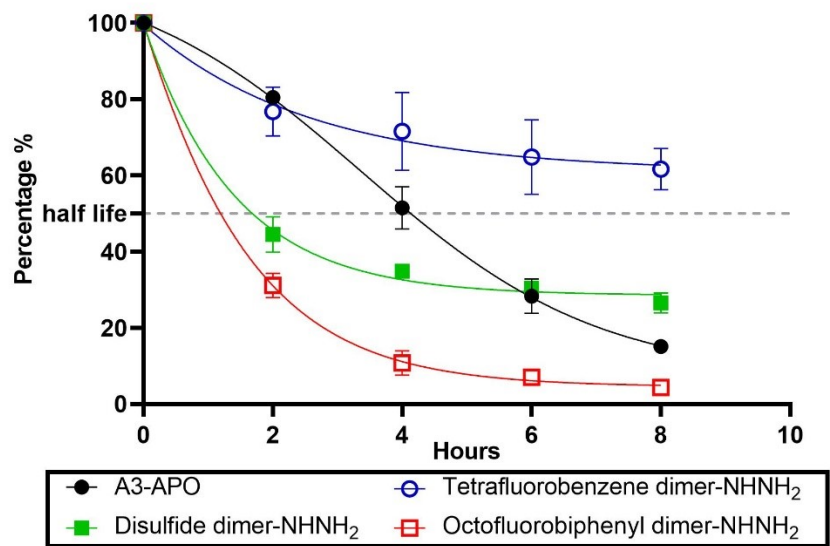


Figure S15. Serum stability of the lead PrAMPs. Note, as the retention time of 4-isopropylbenzyl alcohol is too close to tetrafluorobenzene dimer-NHNH₂ and disulfide dimer-NHNH₂, there was no internal stand in these serum stability mixtures.

Molecular dynamics simulations

The Chex1-Arg20-NH₂ monomer and octofluorobiphenyl dimer-NH₂ peptide structures were firstly simulated in water solution containing approximately 150 mM KCl for 100 ns in order to obtain starting structures for subsequent membrane adsorption and permeation simulations, employing the simulation methodology described below. Parameters for the Chex, hydrazide (-NH₂) and octofluorobiphenyl groups were adapted from those existing for similar chemical entities in the CHARMM36m forcefield, while partial charges for octofluorobiphenyl were estimated using the SwissParam server¹². For each bilayer adsorption simulation, the solution-structure peptide was initially placed approximately 1.0 nm above a pre-equilibrated mixed bilayer composed of palmitoylcholine (POPC) and palmitoylphosphatidylglycerol (POPG) in a 7:3 ratio, which serves as a model of Gram negative inner membranes. The membrane patch had a surface area of 9.23 x 9.23 nm² and was built using the CHARMM-GUI Membrane Builder webserver¹³. Periodic boundary conditions (PBC) were applied, and a simulation box with dimensions of 9.23 x 9.23 x 11.22 nm³ was defined around the peptide-membrane system and solvated with TIP3P water molecules¹⁴, potassium (K⁺) and chloride (Cl⁻) ions to achieve neutrality and an approximate salt concentration of 150 mM. Simulations were performed using GROMACS 2019^{15, 16} and the CHARMM36m forcefield^{17, 18}. The integration time step was set to 2 fs. Van der Waals interactions were switched to zero between 0.8 and 1.2 nm. Electrostatic interactions were evaluated using the fast smooth particle-mesh Ewald (PME) method¹⁹ with a Coulombic potential cut-off of 1.2 nm. Covalent bonds involving hydrogen atoms were constrained using the LINCS algorithm²⁰. For the production simulations, the velocity rescale thermostat of Bussi *et al.*²¹, with a coupling time constant of 0.1 ps, was used to maintain the temperature of all simulations at 310 K. The pressure was maintained at 1 bar using semi-isotropic coupling with the Parrinello-Rahman barostat algorithm²² and a coupling constant of 5 ps. The system was energy minimised using the steepest descent algorithm for a maximum of 10,000 steps. The systems were equilibrated using a series of equilibration simulations according to the protocol specified in the CHARMM-GUI Membrane Builder webserver¹³, in which non-hydrogen atoms were restrained to their initial positions using force constant values of progressively lower values at each equilibration simulation step. Subsequently, 230 ns production equilibrium simulations were performed for each peptide-bilayer system. Following the equilibrium simulations, further 80 ns *non-equilibrium* simulations were performed in which an external force was applied to the membrane-adsorbed peptide to facilitate bilayer penetration. The *umbrella* pulling protocol implemented in GROMACS was employed using a downward pull rate of 0.1 nm per ns. Molecular structures were visualised using Visual Molecular Dynamics version 1.9.3 (VMD)²³.

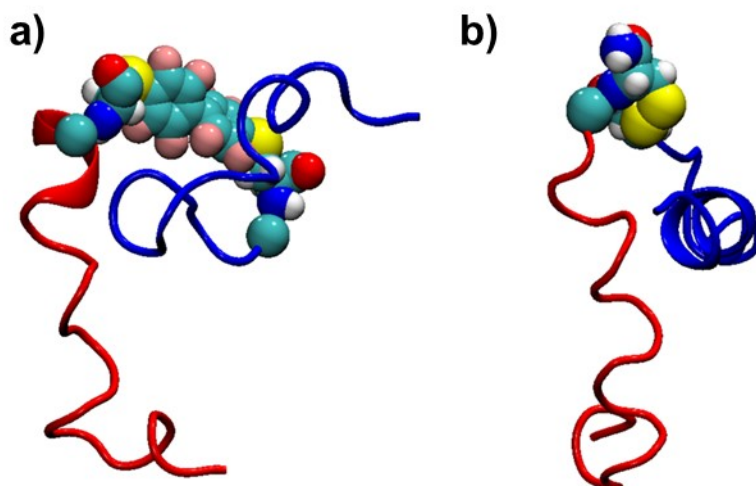


Figure S16. Solution MD simulation final snapshots (at 100 ns) for PrAMP dimers with (a) octofluorobiphenyl linker, and (b) cystine disulfide linker. Ribbons represent peptide backbones, coloured according to chain ID (blue = chain A, red = chain B). Linker atoms are shown as large spheres. The octofluorobiphenyl linker confers greater steric hindrance and structural rigidity to the dimer, resulting in a more extended structure which enables it to adsorb to, and permeate through, membranes with a larger molecular 'footprint', causing a greater degree of bilayer disruption compared to that of the disulfide-linked dimer.

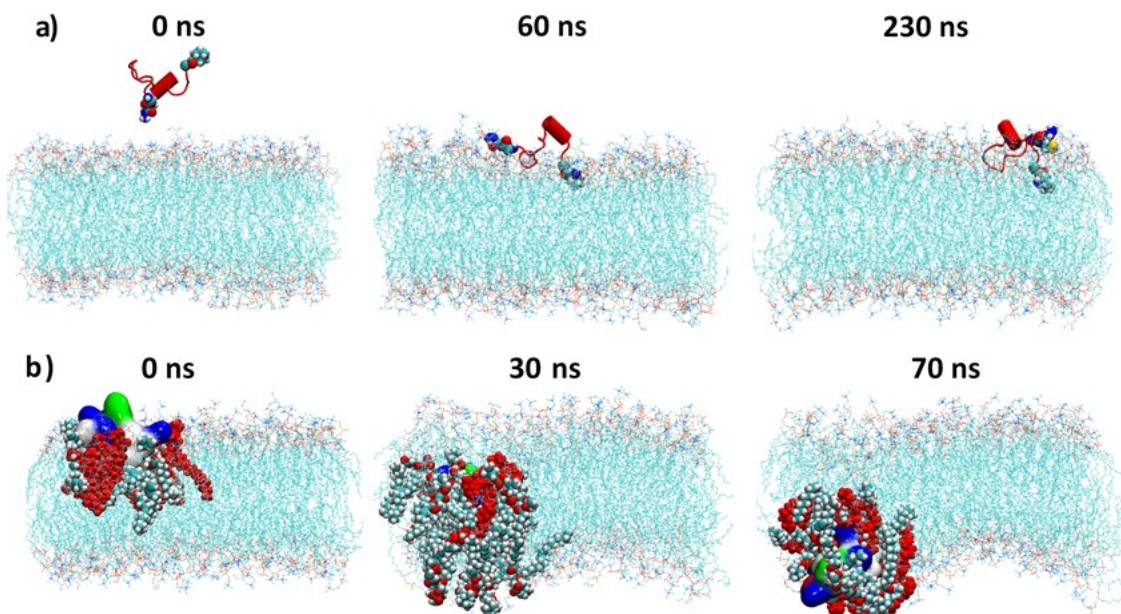


Figure S17. (a) MD simulation snapshots of the initial adsorption of Chex1-Arg20-NH₂ monomer to the model membrane, indicating persistent binding of the peptide to the bilayer surface. The PrAMP backbone is shown as a red ribbon. Chex, hydrazide (-NHNH₂) and octofluorobiphenyl groups are shown as large spheres. The lipids are also shown as ball and stick models, with PG in red. (b) Snapshots of the permeation of Chex1-Arg20-NH₂ monomer into the model membrane, indicating negligible disruption of the lipid chain ordering as the PrAMP enters (30 ns) and exits (70 ns) the bilayer centre. The PrAMP is shown as a surface and colour-coded according to residue charge (blue=Arg, green=neutral polar, white=non-polar).

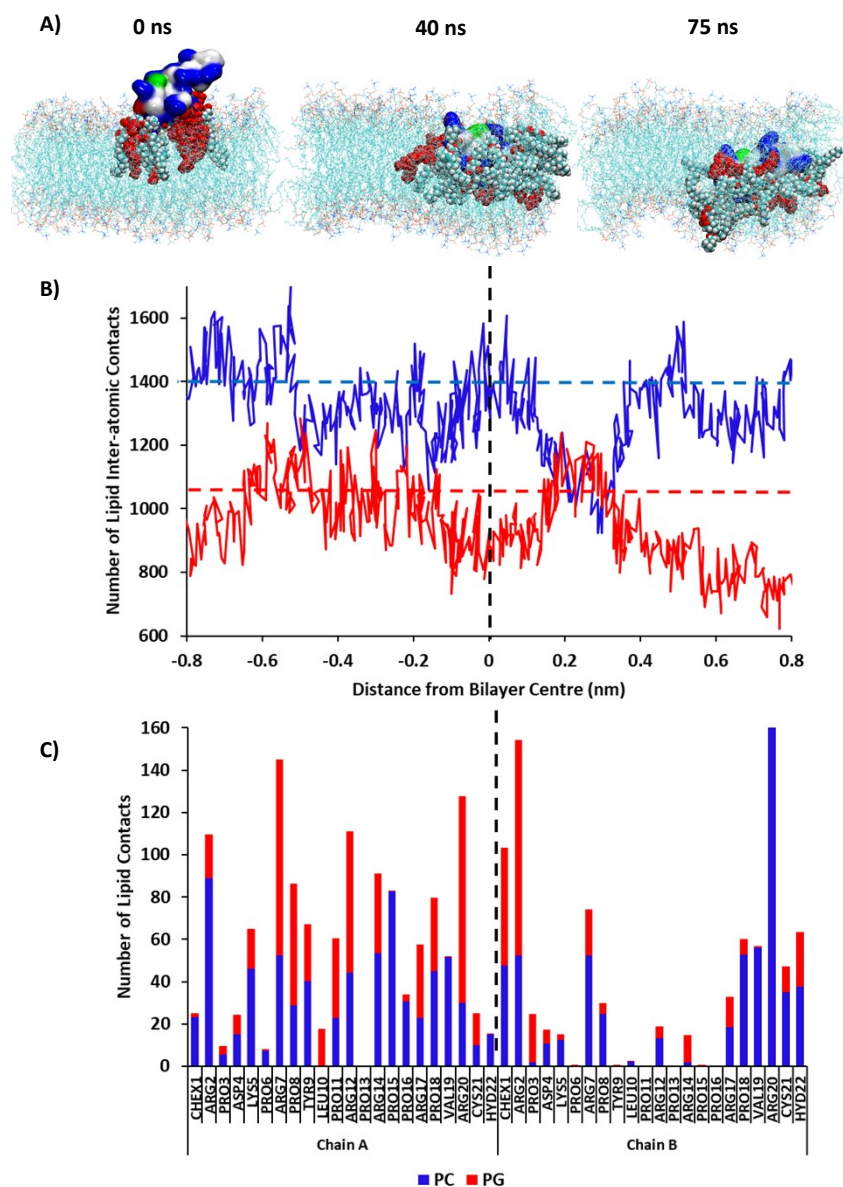


Figure S18. (A) MD simulation snapshots of the permeation of disulfide dimer-NHNH₂ 2 into the model membrane. The PrAMP is shown as a surface and colour-coded according to residue charge (blue=Arg, green=neutral polar, white=non-polar). The annular lipids are also shown as large spheres, with PG in red. (B) Total number of contacts between the PrAMP with PC (blue line) and PG lipids (red line) with respect to approximate position of the peptide centre-of-mass relative to the bilayer centre (dotted black line). For comparison, horizontal dashed lines indicate average contact values for the octafluorobiphenyl-linker dimer-NHNH₂ 7 with PC (horizontal blue dashed line) and PG (horizontal red dashed line) (C) Average numbers of contacts between each PrAMP residue with PC (blue) and PG (red) for each of the two PrAMP chains in the disulfide-dimer during membrane permeation.

SI References

1. W. Li, N. M. O'Brien-Simpson, S. Yao, J. Tailhades, E. C. Reynolds, R. M. Dawson, L. Otvos, M. A. Hossain, F. Separovic and J. D. Wade, *Chem. Eur. J.*, 2017, **23**, 390-396.
2. W. Li, N. M. O'Brien-Simpson, J. Tailhades, N. Pantarat, R. M. Dawson, L. Otvos, Jr., E. C. Reynolds, F. Separovic, M. A. Hossain and J. D. Wade, *Chem. Biol.*, 2015, **22**, 1250-1258.
3. N. M. O'Brien-Simpson, N. Pantarat, T. J. Attard, K. A. Walsh and E. C. Reynolds, *PLoS One*, 2016, **11**, e0151694.
4. W. Li, J. Tailhades, M. A. Hossain, N. M. O'Brien-Simpson, E. C. Reynolds, L. Otvos, F. Separovic and J. D. Wade, *Aust. J. Chem.*, 2015, **68**, 1373-1378.
5. F. H. Waghu, S. Joseph, S. Ghawali, E. A. Martis, T. Madan, K. V. Venkatesh and S. Idicula-Thomas, *Front. Microbiol.*, 2018, **9**, 325.
6. I. M. Helander and T. Mattila-Sandholm, *J. Appl. Microbiol.*, 2000, **88**, 213-219.
7. L. Zhang, P. Dhillon, H. Yan, S. Farmer and R. E. W. Hancock, *Antimicrob. Agents Chemother.*, 2000, **44**, 3317-3321.
8. M.-A. Sani, T. C. Whitwell, J. D. Gehman, R. M. Robins-Browne, N. Pantarat, T. J. Attard, E. C. Reynolds, N. M. O'Brien-Simpson and F. Separovic, *Antimicrob. Agents Chemother.*, 2013, **57**, 3593-3600.
9. N. M. O'Brien-Simpson, W. Li, N. Pantarat, M. A. Hossain, F. Separovic, J. D. Wade and E. C. Reynolds, *Aust. J. Chem.*, 2017, **70**, 220-228.
10. A. Novogrodsky, A. Ravid, A. L. Rubin and K. H. Stenzel, *Proc. Natl. Acad. Sci. U. S. A.*, 1982, **79**, 1171-1174.
11. E. C. Yi and M. Hackett, *Analyst*, 2000, **125**, 651-656.
12. V. Zoete, M. A. Cuendet, A. Grosdidier and O. Michielin, *J. Comput. Chem.*, 2011, **32**, 2359-2368.
13. J. Lee, X. Cheng, J. M. Swails, M. S. Yeom, P. K. Eastman, J. A. Lemkul, S. Wei, J. Buckner, J. C. Jeong, Y. Qi, S. Jo, V. S. Pande, D. A. Case, C. L. Brooks, A. D. MacKerell, J. B. Klauda and W. Im, *J. Chem. Theory Comput.*, 2016, **12**, 405-413.
14. W. L. Jorgensen, J. Chandrasekhar, J. D. Madura, R. W. Impey and M. L. J. T. J. o. c. p. Klein, *The Journal of chemical physics* 1983, **79**, 926-935.
15. D. Van Der Spoel, E. Lindahl, B. Hess, G. Groenhof, A. E. Mark and H. J. Berendsen, *J. Comput. Chem.*, 2005, **26**, 1701-1718.
16. S. Pronk, S. Pall, R. Schulz, P. Larsson, P. Bjelkmar, R. Apostolov, M. R. Shirts, J. C. Smith, P. M. Kasson, D. van der Spoel, B. Hess and E. Lindahl, *Bioinformatics*, 2013, **29**, 845-854.
17. J. Huang, S. Rauscher, G. Nawrocki, T. Ran, M. Feig, B. L. de Groot, H. Grubmuller and A. D. MacKerell, Jr., *Nat Methods*, 2017, **14**, 71-73.
18. J. Huang, S. Rauscher, G. Nawrocki, T. Ran, M. Feig, B. L. de Groot, H. Grubmüller and A. D. MacKerell, *Nat. Methods*, 2017, **14**, 71-73.
19. U. Essmann, L. Perera, M. L. Berkowitz, T. Darden, H. Lee and L. G. J. T. J. o. c. p. Pedersen, *The Journal of chemical physics*, 1995, **103**, 8577-8593.
20. B. Hess, H. Bekker, H. J. C. Berendsen and J. G. E. M. Fraaije, *J. Comput. Chem.*, 1997, **18**, 1463-1472.
21. G. Bussi, D. Donadio and M. J. T. J. o. c. p. Parrinello, *The Journal of chemical physics*, 2007, **126**, 014101.
22. M. Parrinello and A. J. J. o. A. p. Rahman, *J. Appl. Phys.*, 1981, **52**, 7182-7190.
23. W. Humphrey, A. Dalke and K. J. J. o. m. g. Schulten, *J. Mol. Graph.*, 1996, **14**, 33-38.